Size dependent Cu dielectric function for plasmon spectroscopy: Characterization of colloidal suspension generated by fs laser ablation

J. M. J. Santillán, F. A. Videla, M. B. Fernández van Raap, D. C. Schinca, and L. B. Scaffardi

Related Articles

Particle size and density of a slurry from ultrasonic backscattering measurements at a solid interface
Rev. Sci. Instrum. 83, 095101 (2012)

Tuning effective interactions close to the critical point in colloidal suspensions
J. Chem. Phys. 137, 084903 (2012)

A method to measure specific absorption rate of nanoparticles in colloidal suspension using different configurations of radio-frequency fields
Appl. Phys. Lett. 101, 083118 (2012)

Krylov subspace methods for computing hydrodynamic interactions in Brownian dynamics simulations
J. Chem. Phys. 137, 064106 (2012)

Effective dielectric constant of two phase systems: Application to mixed conducting systems
J. Appl. Phys. 112, 034107 (2012)
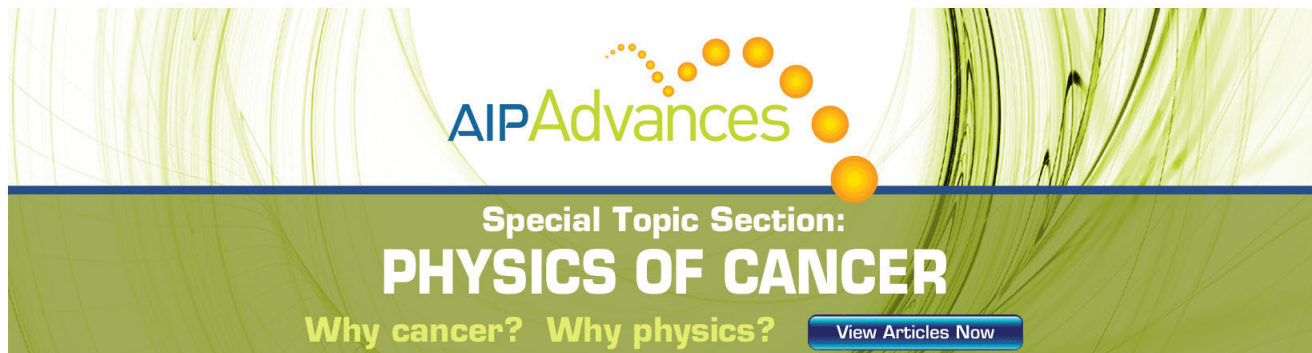
Additional information on J. Appl. Phys.

Size dependent Cu dielectric function for plasmon spectroscopy: Characterization of colloidal suspension generated by fs laser ablation

J. M. J. Santillán,[1] F. A. Videla,[1,2] M. B. Fernández van Raap,[3] D. C. Schinca,[1,2,a)] and L. B. Scaffardi[1,2]

[1]*Centro de Investigaciones Ópticas (CIOp), (CONICET La Plata - CIC), Argentina*
[2]*Departamento de Ciencias Básicas, Facultad de Ingeniería, UNLP, Argentina*
[3]*Departamento de Física-IFLP, Universidad Nacional de La Plata-CONICET, CIOp CC3 (1897) Gonnet, La Plata, Argentina*

Copper metal nanoparticles (Nps) have received increasing interest during the last years due to their potential applications in several fields of science and technology. Their optical properties depend on the characteristics of the dielectric function of the metal, their size, and the type of environment. The contribution of free and bound electrons on the dielectric function of copper Nps is analyzed as well as their influence on its plasmonic properties. The contribution of free electrons is corrected for particle size under 10 nm, introducing a term inversely proportional to the particle's radius in the damping constant. For bound electron contribution, interband transitions from the d-band to the conduction band are considered. For particles with sizes below 2 nm, the larger spacing between electronic energy levels must be taken into account by making the electronic density of states in the conduction band size-dependent. Considering these specific modifications, optical parameters and band energy values could be determined by fitting the bulk complex dielectric function. The obtained values were coefficient for bound electron contribution $K_{bulk} = 2 \times 10^{24}$, gap energy $E_g = 1.95$ eV, Fermi energy $E_F = 2.15$ eV, and bound electrons damping constant $\gamma_b = 1.15 \times 10^{14}$ Hz. Based on the dielectric function determined in this way, experimental extinction spectra of colloid suspensions generated by ultrafast laser ablation of a solid copper target in liquids was fitted using the Drude-interband model and Mie's theory. Depending on the experimental conditions and liquid medium, the particles in the suspension may have nanometric or subnanometric core size and may be capped with a shell of oxide. From the fitting, it was possible to determine the structure and size distribution of spherical bare core and core-shell copper Nps in the nanometer-subnanometer size range. These results were compared with those obtained by standard microscopy techniques such as AFM and HRTEM. There is a very good agreement between the three techniques, showing that optical extinction spectroscopy (OES) is a good complementary technique to standard high resolution electron microscopy and AFM for sizing spherical nanometric-subnanometric Nps. OES has also the advantage of a very good measurement statistics, due to the large number of probed particles across the sample cell. Besides, it avoids coalescence effects since the measurement is made directly on the colloidal suspension. © *2012 American Institute of Physics.* [http://dx.doi.org/10.1063/1.4751328]

I. INTRODUCTION

The study of copper metal Nps is an area of active research due to their wide potential applications in chemistry, catalysis, material science, and nanofluidics.[1–4] The high conductivity, large extinction cross section, photosensitivity, and low cost of copper make it a promising material for the development of miniaturized devices that can integrate electronic, photonic, and chemical features for use in biological nanosensors.[5–9] It is also interesting its capability of insertion in host polymer matrices for nonlinear optics applications.[10–12]

The spectral characteristics of plasmons of metal Nps may be used to characterize the size of noble metal Nps in the range of 10–100 nm radius.[13] Recently, we have shown a method for sizing gold and silver nanoparticles below 10 nm by fitting extinction spectra with Mie's theory together with a conveniently modified bulk dielectric function.[14–18] This modification considers that the damping constant in Drude's model is increased due to additional collisions of free electrons with the boundary of the particle. This fact produces a size dependence of the dielectric function and consequently of the refractive index. For noble metals, transitions of bound electrons to conduction band levels contribute appreciably to the dielectric function. For silver and gold, Pinchuk *et al.*[19] analyzed the influence of interband electronic transitions on the frequency, amplitude, and bandwidth of the surface plasmon resonance in small metal clusters in the Rayleigh approximation. However, for the case of copper Nps, the influence of free and bound electrons on the dielectric function and its dependence with size has not been fully analyzed.

This work consists of two parts: the first one is devoted to study the size effect on the dielectric function of copper in order to analyze its influence on the extinction spectra. Both free and bound electron contributions will be considered,

a)Electronic mail: daniels@ciop.unlp.edu.ar.

and the values of the different parameters involved in the model will be determined.

The second part is devoted to the application of this technique to retrieve the size distribution of colloidal copper suspensions generated by fs laser ablation in liquid media, as well as the possible appearance of core-shell copper-copper oxide structure.

II. THEORETICAL FRAMEWORK

The complex dielectric function for bulk metals can be decomposed into two additive terms as a function of frequency of the electromagnetic wave ω: a free-electron contribution and an interband (or bound-electron) contribution. When the metal particle has nanometric size, the dielectric function also depends on the particle radius R and it can be written as

$$\varepsilon_{size}(\omega, R) = \varepsilon_{bound-electrons}(\omega, R) + \varepsilon_{free-electrons}(\omega, R). \quad (1)$$

For bound electrons, the complex dielectric function arising due to transitions from the copper d-band to the conduction sp-band can be calculated using the expression given by Inouye *et al.*[20] and modified to take into account the increasing spacing of the energy levels when the particle size decreases[14]

$$\varepsilon_{bound-electrons}(\omega, R) = K_{bulk} \left(1 - \exp\left(-R/R_0\right) \right)$$
$$\int_{\omega_g}^{\infty} \frac{\sqrt{x - \omega_g}}{x} [1 - F(x, T)] \frac{(x^2 - \omega^2 + \gamma_b^2 + i\, 2\,\omega\,\gamma_b)}{(x^2 - \omega^2 + \gamma_b^2)^2 + 4\,\omega^2\gamma_b^2} \, dx,$$
$$(2)$$

where $\hbar\omega_g$ is the copper gap energy (E_g), $F(x, T)$ is the Fermi energy distribution function of conduction electrons of energy $\hbar x$ at the temperature T with Fermi energy E_F, γ_b represents the damping constant of the interband transition, $R_0 = 0.35$ nm is a scale factor, and K_{bulk} is a proportionality constant.

The size dependence introduced in the factor K_{bulk} $\left(1 - \exp\left(-R/R_0\right) \right)$ follows the idea introduced by Logunov *et al.*[21] that the electronic density of states is different for nanoparticles of different sizes. These authors conclude that small particles have larger spacing between electronic states, so the density of states will be smaller for very small Nps.

For free electrons, the complex dielectric function can be written as

$$\varepsilon_{free-electrons}(\omega, R) = 1 - \frac{\omega_p^2}{\omega^2 + i\left(\gamma_{bulk} + C\frac{v_F}{R}\right)\omega}, \quad (3)$$

where ω_p is the bulk plasma frequency and the term in parenthesis in the denominator is the size modification of the free-electron damping constant, being γ_{bulk} the bulk damping constant in the Drude model, v_F the Fermi velocity, and C a constant that depends on the electron scattering processes inside the nanoparticle.

With the dielectric function written in this way, it is possible to fit the experimental bulk dielectric function

measured by Johnson and Christy.[22] For this purpose, we have set the radius R equal to a sufficiently large value with respect to R_0 to ensure the bulk regime condition. In our case, $R = 100$ nm was used. For the theoretical calculations of Eqs. (1)–(3), the value for $\omega_p = 13.4 \times 10^{15}$ Hz was taken from Ref. 23, and the free electron damping constant $\gamma_{bulk} = 1.45 \times 10^{14}$ Hz from Ref. 22. Fermi velocity for copper was taken from Ref. 24 to be $v_F = 15.7 \times 10^{14}$ nm/s. C values range between 0.5 and 1.2, as derived from first principles calculations.[25] In our case, a C value of 0.8 was used.

The simultaneous fit of the real and imaginary parts of both contributions yields the optimum values of K_{bulk}, E_g, E_F, and γ_b which are included in Table I. Using this model, these parameters were determined for the first time in this work.

Figures 1(a) and 1(b) show the real and imaginary components of bound (Eq. (2)) and free electron (Eq. (3)) contributions calculated separately, while its sum (full line) is the best fit to experimental bulk values derived from complex refractive index data taken from Johnson and Christy[22] (represented by full squares).

It is interesting to notice from Figure 1(b) that the bound electron contribution dominates over the free electron contribution for wavelengths shorter than 600 nm. We will see in the following section that the interband transitions influence the behaviour of copper Np optical extinction spectrum in the short wavelength range.

Figure 2 shows the behaviour of the real and the imaginary parts of the total dielectric function (Eq. (1)) as a function of wavelength for different Np radii.

It can be seen that the real part of the dielectric function (Fig. 2(a)) is very sensitive to size for $R < 2$ nm. However, this sensitivity decreases for the range 2–10 nm and it is almost coincident with the bulk curve for $R = 10$ nm. On the other hand, the imaginary part (Fig. 2(b)) shows a similar limit behaviour for $R > 15$ nm, but there seems to be also a limiting behaviour for $R = 0.6$ nm.

The K_{bulk}, E_g, E_F, and γ_b parameters that appear in Eq. (2) influence independent features in the experimental dielectric function. As an example, we show in Figs. 3–5 the modifications on the complex dielectric function due to small changes in E_g, E_F, and γ_b, respectively. Figure 3 shows the influence of E_g on the complex dielectric function. Although the real part (Fig. 3(a)) seems insensitive to changes in E_g, there is an observable difference in the calculated curves for the imaginary part (Fig. 3(b)), especially in the wavelength region between 350 and 530 nm (region I), corresponding to the onset of the gap transition.

Figure 4 shows the influence of E_F on the complex dielectric function. It can be seen that for small variations in

TABLE I. Optical parameters for bulk copper determined in this work.

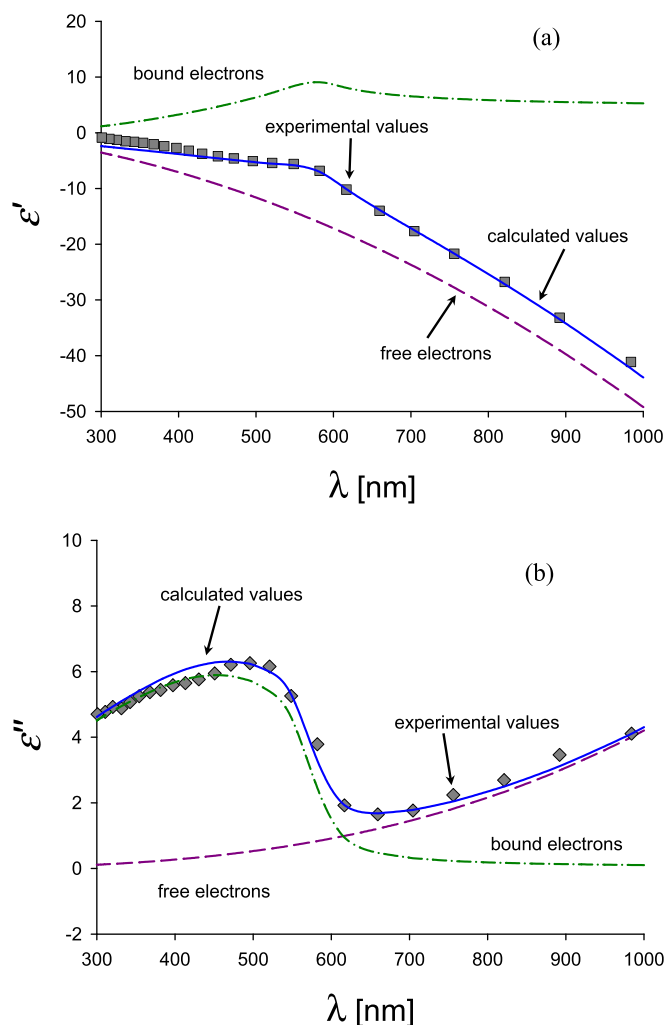| Parameter	Symbol	Value
Coefficient for bound electron contribution	K_{bulk}	2×10^{24}
Gap energy	E_g	1.95 eV
Fermi energy	E_F	2.15 eV
Damping constant for bound electrons	γ_b	1.15×10^{14} Hz

FIG. 1. Comparison between experimental bulk values (squares and diamonds) and theoretical calculation for the real and imaginary part of copper dielectric function. Experimental values were derived from Johnson and Christy[22] while theoretical free and bound electron contributions to the complex dielectric function were carried out using Eqs. (1)–(3). (a) Real component ε' and (b) imaginary component ε''. Determined parameters are given in Table I.
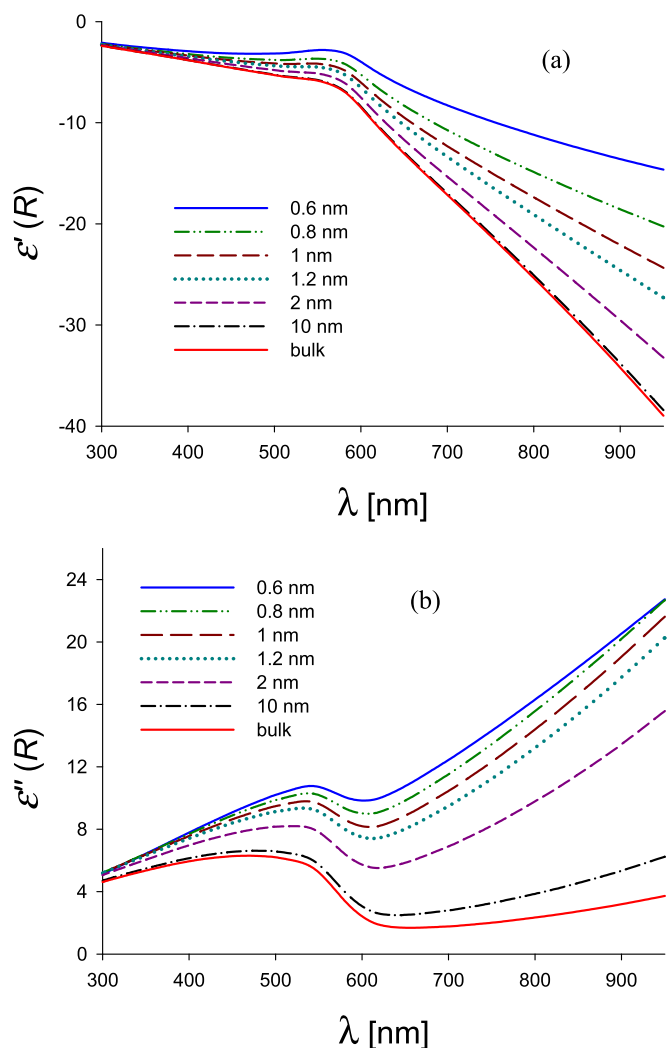

FIG. 2. Real (a) and imaginary (b) parts of the copper complex dielectric function considering free and bound electron contributions for different values of Np radii.

the value of E_F, the real part (Fig. 4(a)) shows almost no changes. However, the most prominent changes occur for the imaginary part (Fig. 4(b)) between 530 and 700 nm (region II), which corresponds to the edge transition. This region is different and independent from that in which the influence of E_g is more noticeable.

Finally, Fig. 5 shows the influence of small variations of γ_b over the real and the imaginary part of the dielectric function. Here again, while the real part (Fig. 5(a)) is almost insensitive to changes in γ_b, the imaginary part (Fig. 5(b)) shows a stretching around the midpoint at 570 nm.

Considering the independent influence of these parameters, it was possible to use them to fit the experimental bulk dielectric function and hence obtain the optimum values shown in Table I. Knowledge of the size dependent dielectric function will be used for calculating the theoretical extinction cross section to fit the experimental extinction spectra of colloidal suspension.

III. EXPERIMENTAL PROCEDURE

Copper Nps were fabricated by ultrafast pulse laser ablation in liquids. A high purity grade 1 mm thick copper circular disk was used to carry out these experiments. Laser ablation was performed using a Ti:Sapphire chirped pulsed amplification (CPA) system from Spectra Physics, emitting pulses of 100 fs width at 1 kHz repetition rate centered at 800 nm wavelength. The maximum output energy was 1 mJ per pulse. A 5 cm focal length was used to focus the laser beam on the target disk surface, which was immersed in water or acetone. The energy per pulse used in this experiment was 500 μJ. The fabrication process was done during 20 min, after which the solution shows a typical greenish colour in water or reddish in acetone, which is attributed to the presence of a large number of Nps in the solution. Optical extinction spectroscopy was conducted by means of a Shimadzu spectrophotometer from 300 to 1000 nm. Measurements were performed on highly diluted and sonicated Nps solutions immediately after laser ablation. Since many other authors work with laser ablation in pure liquids, no
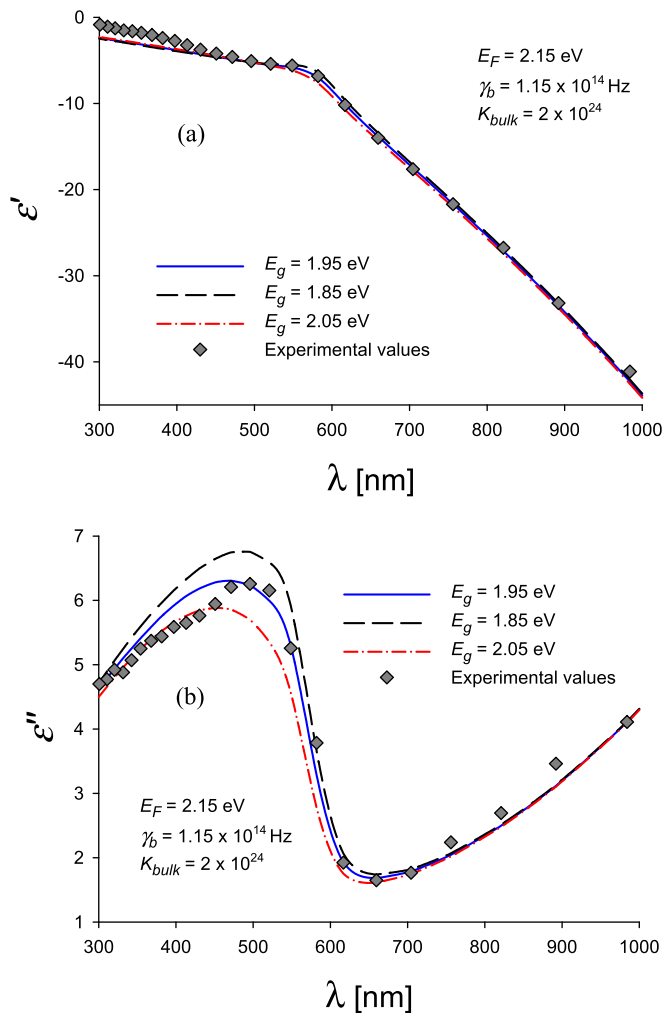
FIG. 3. Influence of E_g on the complex dielectric function: (a) real component and (b) imaginary component. The influence of the imaginary part is more noticeable for wavelengths in the range 350–530 nm (region I).

FIG. 4. Influence of E_F on the complex dielectric function: (a) real part and (b) imaginary part. The influence on the imaginary part is more noticeable between 500 and 750 nm (region II).

surfactants were added to the sample to make the analysis in pure water or acetone without extra additives.

The mechanisms underlying the formation of copper Nps with pulsed laser ablation of a copper solid target in liquids are very complex. The formation mechanism includes several reactions in nonequilibrium high-temperature high-pressure plasma-liquid environment. The shockwave that results from the laser breakdown generates these conditions at the liquid-plasma interface, which becomes an active chemical reaction zone that enhances the bonding of copper species with ionized water molecules to form copper oxide Nps. These conditions encountered at the solid target-liquid interface dominate the size and structural phase of the synthesized Nps. The Cu clusters formed after the adiabatic expansion (and cooling) of the plasma plume react with the solvent (hydroxyl radicals or oxygen atoms) and may produce copper oxides around bare Cu particles.

To study the composition of the colloidal suspension, the samples were analyzed using atomic force microscopy (AFM) imaging. The colloidal suspensions obtained by laser ablation were highly diluted and drop coated on scratch free high quality mica Ruby Mica Disc (average roughness of 0.073 nm). The observations were carried out onto the dried
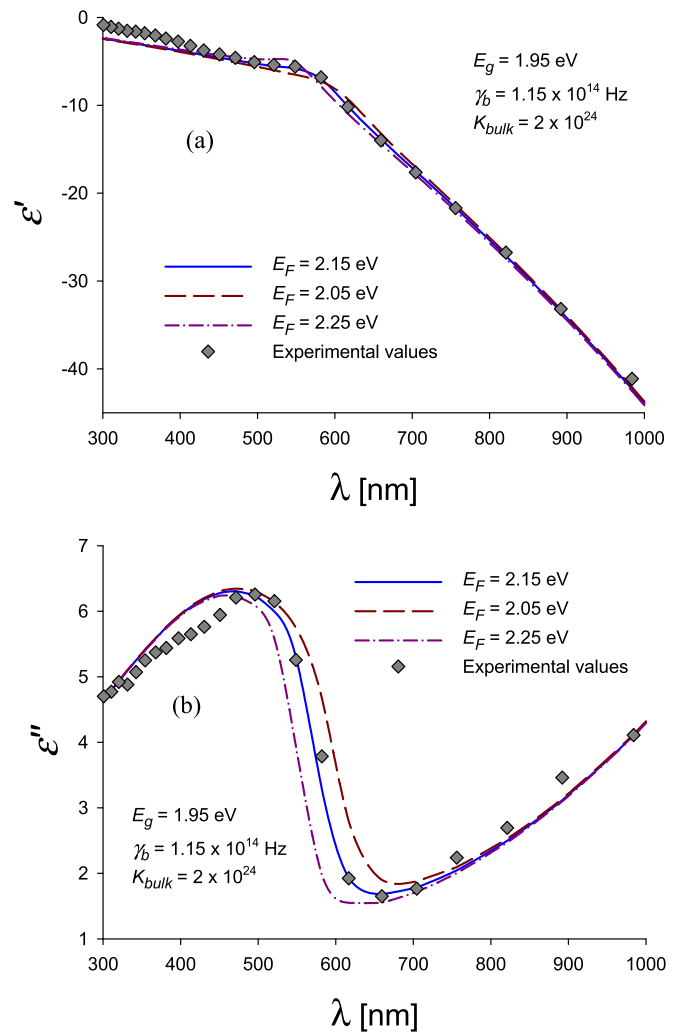
sample with a NT-MDT Solver Pro microscope (minimum scanning step of 0.006 nm in vertical direction) working at semicontact mode using a triangular NSG20 cantilever (resonance frequency 534 kHz) with sharp tip of 10 nm curvature radius. On the other hand, HRTEM (JEOL 4000EX high-resolution) images were also obtained for colloidal suspensions in water and acetone.

IV. RESULTS

Since the size of the copper Nps considered in this paper is very small compared with the incident wavelength, the response to optical extinction can be described using the electrostatic approximation. In this approach, the expression for the extinction cross section is

$$C_{ext.} = k' \, \text{Im}(\alpha), \qquad (4)$$

where α is the polarizability, $k' = \frac{2\pi n_m}{\lambda}$ is the wavenumber in the medium surrounding the particle, n_m is the refractive index of the medium, and λ is the wavelength of the incident light in vacuum.

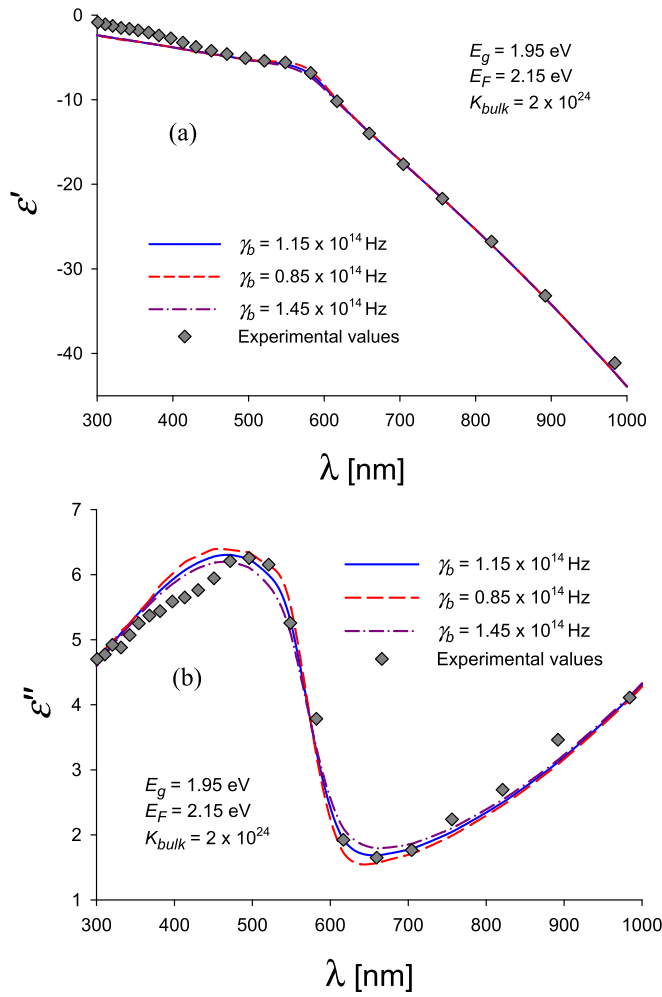Since during ablation there are conditions of high temperature and high pressure in the plasma plume, oxidation

FIG. 5. Influence of γ_b on the complex dielectric function: (a) real part and (b) imaginary part. There is a stretching around 570 nm that affects mainly the peak and the valley.
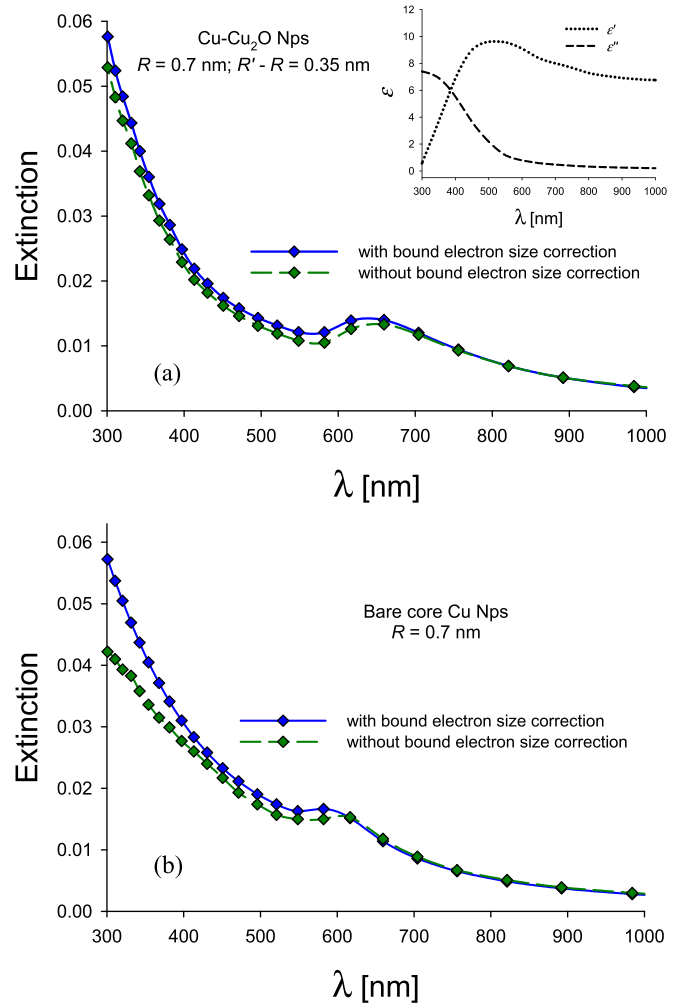

FIG. 6. Extinction coefficient for (a) core-shell Cu-Cu$_2$O Np and (b) bare core Cu Np, with and without bound electron size correction. The difference in the spectra is more noticeable for wavelengths smaller that the plasmon peak, where the influence of the bound electron is more important.

processes proceed very fast over the formed copper Nps, and there is a large probability that copper-copper oxide Nps may be generated. In view of this, it is important to take into account the expression of the polarizability for capped particles. So, for spherical Nps with core-shell structure, the polarizability can be written as[26]

$$\alpha = 4\pi R'^3 \frac{(\varepsilon_2 - \varepsilon_m)(\varepsilon_1 + 2\varepsilon_2) + f(\varepsilon_1 - \varepsilon_2)(\varepsilon_m + 2\varepsilon_2)}{(\varepsilon_2 + 2\varepsilon_m)(\varepsilon_1 + 2\varepsilon_2) + f(2\varepsilon_2 - 2\varepsilon_m)(\varepsilon_1 - \varepsilon_2)},$$
(5)

where $f = \left(\frac{R}{R'}\right)^3$ is the ratio between inner and outer radius volumes, $R = r_{core}$ is the metal central core (copper), $R' = r_{(core+coating)}$ is the outer radius (copper core + copper-oxide coat thickness), $\varepsilon_1 = \varepsilon_1(\lambda, R)$, $\varepsilon_2 = \varepsilon_2(\lambda)$, and $\varepsilon_m = \varepsilon_m(\lambda)$ are the dielectric functions of the core, coating (shell), and surrounding medium, respectively. Another parameter related with the extinction cross section is the extinction coefficient defined as $Q_{ext} = C_{ext}/\pi R'^2$.

Data for ε_1 was derived from Ref. 22, while the complex dielectric function ε_2 corresponding to the Cu$_2$O shell was taken from Palik.[27]

Figure 6(a) shows the extinction coefficient for a core-shell Cu-Cu$_2$O Np for a subnanometric metal radius $R = 0.7$ nm covered by a thin layer of copper-oxide (R'-R $= 50\% R$), calculated with and without bound electron size correction. It can be observed that the peak position is near 650 nm for both spectra, but differences are more noticeable for wavelengths lower than 650 nm, where the influence of imaginary part of bound electrons is more important. The correction of bound electron smooths the contrast $(I_{max} - I_{min})/I_{max}$ in the mentioned range, while for larger wavelengths the spectra are coincident. The inset show the real and imaginary parts of the complex dielectric function of Cu$_2$O.

Figure 6(b) shows the extinction coefficient for a subnanometric copper bare core, which is a special case of core-shell Np where $R' = R$. Here, the differences between the spectra are more evident for wavelengths shorter than 600 nm, and the plasmon resonance is blue shifted from 650 nm (with oxide shell) to a small shoulder at 600 nm without shell.

We may apply the above calculations to fit the experimental extinction spectra of the obtained suspension. Figure 7
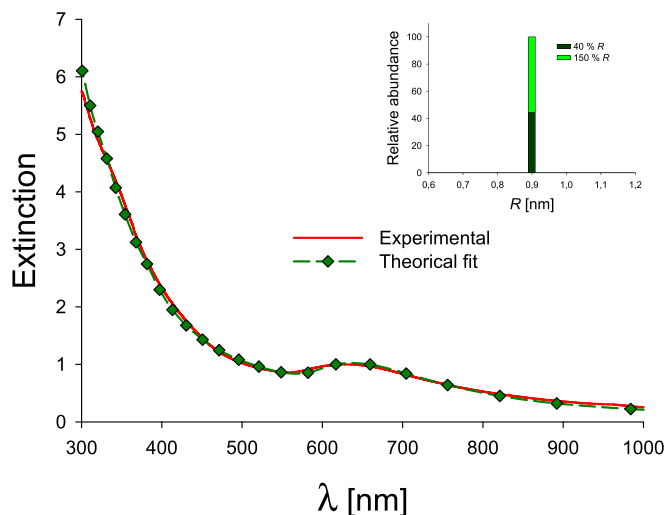
FIG. 7. Solid line corresponds to normalized experimental spectral extinction of Cu-Cu$_2$O Nps fabricated in water by laser ablation with 500 μJ pulse energy. Dashed line and points shows the best fit calculated theoretically with a bimodal contribution for core-shell Cu-Cu$_2$O Np: (1) $R = 0.9$ nm and R'-$R = 0.36$ nm and (2) $R = 0.9$ and R'-$R = 1.35$ nm. The abundance for the first contribution is 0.45 and 0.55 for the second.

shows the best fit of the experimental extinction spectrum corresponding to a colloidal suspension fabricated by fs laser ablation. The fit was attained considering a linear combination of two types of core-shell Nps: one with 0.9 nm core radius and shell thickness of 40% R and the other of the same core radius and a 150% R shell thickness. The coefficients of this combination, 0.45 and 0.55, respectively, give the optimum relative abundance of the species. No combination of bare core particles could fit the whole spectrum.

It is interesting to notice also that neither of the single species can fit the whole spectrum by itself. This fact can be seen in Figure 8 where the normalized spectrum of each species is represented together with the experimental spectrum for comparison. It can be seen that the 40% shell thickness
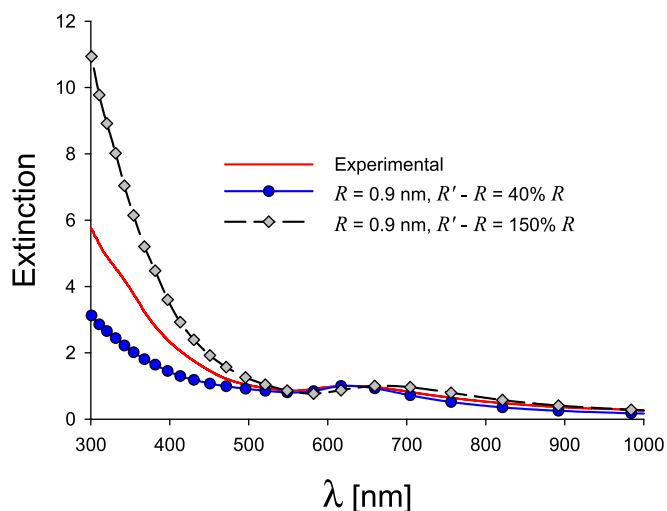
curve correctly fits the plasmon peak position, but there is a serious disagreement for wavelengths shorter than 550 nm. The 150% shell thickness curve has its peak position shifted to the IR in about 60 nm with respect to the experimental one, a shift that can be readily measurable with a commercial spectrophotometer and does not fit correctly the spectrum in the short wavelength range.

Changes in core radius of ± 0.1 nm or in shell thickness of $\pm 20\%$ make impossible to fit the experimental curve for wavelengths shorter than 600 nm. This fact shows the good sensitivity of the fitting procedure.

Similar results were obtained using other liquid as the host medium. Figure 9 shows the experimental curves (red full line) and the theoretical fit (full diamond and dashed line) corresponding to copper Nps in acetone fabricated with 500 μJ. The optimum size distribution has a dominant size of Cu bare core 2 nm radius and includes a 7% abundance of 4 nm radius and a 14% abundance of 10 nm radius of Cu-Cu$_2$O Nps. There is also an important subnanometric contribution of 0.8 nm core radius of the same configuration whose abundance is 32%. It is important to remark the fact that core radii and shell thicknesses that appear in the histogram depicted in the inset indicate a bimodal distribution composed by small radii in the range 1 to 4 nm and a larger one centered at 10 nm.

To compare the sizing results obtained with the OES method, we performed microscopy analyses on the same colloidal samples. Figure 10(a) shows, as an example, an AFM picture of the colloidal sample generated in water using 500 μJ pulse energy laser ablation. Individual particles were clearly resolved by AFM imaging of the scanned 1.2 μm $\times$ 1.2 μm area under the low concentration condition used. It is well known that tip curvature radius limits lateral resolution, but height measurements have larger resolution and can retrieve NP size with higher accuracy. The height profiles of line 1 and line 2 in the upper panel of Figure 10(a) are shown in the lower panel. The scan of the first line
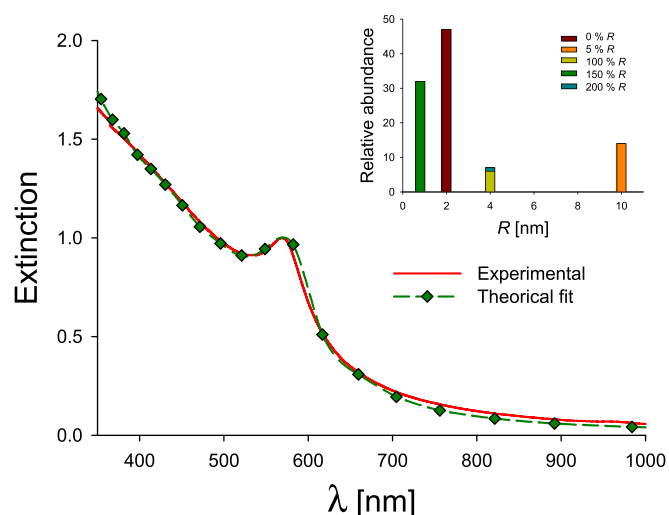

FIG. 8. Solid line corresponds to experimental spectral extinction of Cu-Cu$_2$O Nps fabricated by laser ablation with 500 μJ energy. Squares with full line is calculated extinction spectrum corresponding to $R = 0.9$ nm and R'-$R = 40\%$ R. Circles with dashed line is calculated extinction spectrum corresponding to $R = 0.9$ nm and R'-$R = 150\%$ R.

FIG. 9. Experimental spectra and theoretical fit of colloidal suspension in acetone: (a) pulse energy E $= 500$ μJ. The fit is based on a combination of Cu bare core and Cu-Cu$_2$O structures.
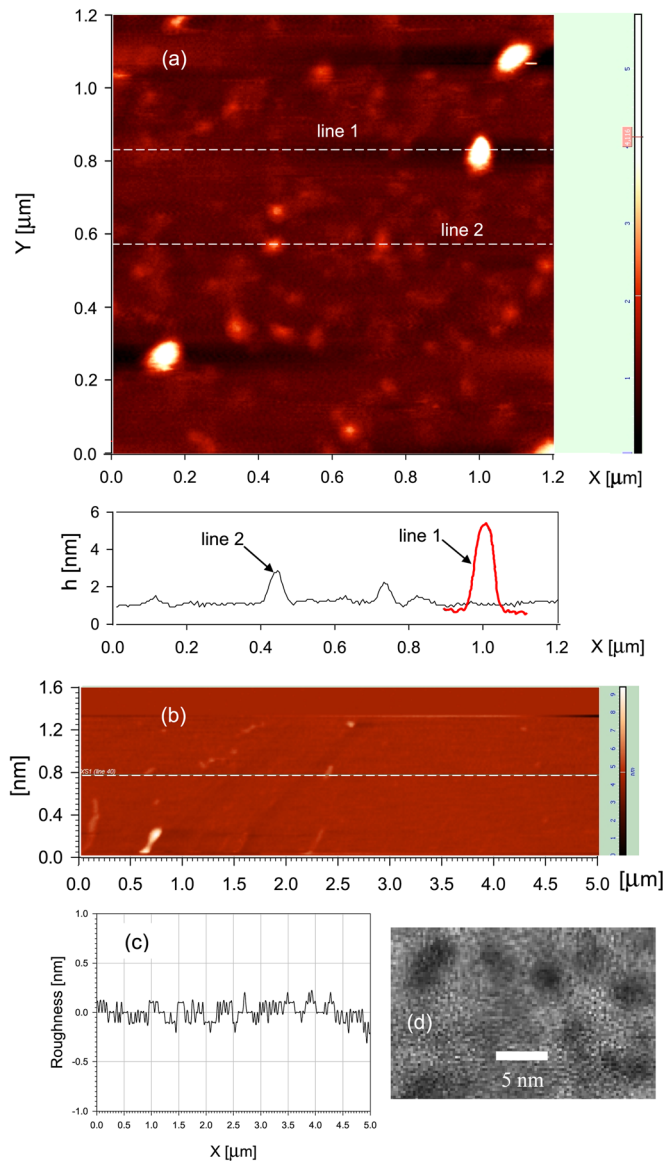
FIG. 10. (a) AFM image of the diluted colloidal suspension obtained by laser ablation with 500 μJ pulse energy (upper panel) and height (diameter) of the NPs vs X position for line 1 and line 2 marked on AFM image(lower panel). Notice the single peak in line 1 and two single Np peaks in line 2. (b) AFM image of the mica substrate. (c) Measured roughness profile of the mica substrate shows an average value of 0.07 nm. (d) HRTEM image of core-shell Cu-Cu$_2$O nanoparticles. The external radii observed are in good agreement with the values obtained by the AFM image and extinction spectroscopy.

in the range $0.9\,\mu m < x < 1.1\,\mu m$ includes a single Np of 4.5 nm height (diameter). This size agrees with the results obtained by extinction spectroscopy of the same sample considering a core-shell Cu-Cu$_2$O particle with a core radius of 0.9 nm and a shell thickness of 1.35 nm. On the other hand, line 2 scans over a 2.2 nm height Np, which agrees with the other size present in the core-shell Cu-Cu$_2$O colloidal suspension of Figure 7 and derived from the fitting of its extinction spectrum. To stress the reliability of these results, Figures 10(b) and 10(c) show the image and roughness profile of the mica substrate over which the colloidal suspension was deposited. Mica substrate average roughness of 0.07 nm (Figure 10(c)) is almost two orders of magnitude smaller

than the Nps under inspection, which ensures a very good contrast ratio between particles and background. Finally, Figure 10(d) shows an HRTEM image of the same colloidal suspension. It can be seen that there are several nanoparticles showing a central dark core and a light gray region surrounding the core evidencing core-shell Cu-Cu$_2$O Nps. The external radii of the core-shell Nps between 1.5 nm and 2.5 nm agree with the values determined by AFM microcopy and extinction spectroscopy.

A similar analysis and comparison between extinction spectroscopy and AFM/HRTEM was carried out for the colloidal samples in acetone. The results between the three methods showed very good agreement.

All these results support the fact that OES is a very simple, inexpensive, and sensitive technique to size nanometric-subnanometric bare core or core-shell Nps colloids. The results derived from extinction spectroscopy are consistent with those obtained by standard techniques such as electron microscopy and atomic force microscopy. Besides, the measurement statistics for OES is very large, with typical values ranging from 10^{12} to 10^{14} Nps, a fact that enhances the reliability of the measurements.

V. CONCLUSIONS

This work was focused on two aspects of copper Nps characterization. The first one dealt with the analysis of the behaviour of free and bound electron contribution to the wavelength dependent dielectric function of copper. The free electron contribution was modified as usual including a term inversely proportional to the particle radius in the expression of the bulk damping constant. With this modification, both real and imaginary parts of the free electron dielectric function show a noticeable dependence with size from 1 nm to 10 nm, with a limiting behaviour to bulk for a radius $R \approx 10$ nm. The bound electron contribution of transitions from the d-band to the conduction band was modelled using an expression that takes into account all the possible interband transitions. The parameters involved in the expression for the bulk bound electron dielectric function, such as K_{bulk}, E_g, γ_b, and E_F, were adjusted to fit simultaneously the real and imaginary experimental values for bulk copper complex dielectric function taken from Johnson and Christy.[22] For subnanometric Nps, a size dependence factor that accounts for the larger energy level spacing was included in the former expression for the bound electron dielectric function. This correction is important from subnanometric size to a radius of about 2 nm, above which the correction is negligible.

The second part of the work was devoted to the application of this technique to retrieve the size distribution of colloidal copper suspensions generated by fs laser ablation in water and acetone, as well as the possible appearance of core-shell copper-copper oxide structure. The expressions of the obtained dielectric function were used in the calculation of the polarizability of metal Nps within Mie's theory, showing the influence of bound electron size correction on the shape of the extinction spectrum of subnanometric Nps. For core-shell Cu-Cu$_2$O Nps, the differences are more noticeable for wavelengths between 300 nm and 750 nm

(regions I and II), where the influence of imaginary part of bound electrons is more important. For the case of bare core Cu Nps, the differences between the spectra with and without size correction are more evident for wavelengths shorter than 600 nm, where the influence of the bound electrons is more important.

As an example of these theoretical studies, we have successfully fitted the experimental optical extinction spectra of core-shell Cu-Cu$_2$O Nps fabricated by ultrashort pulse laser ablation of solid target in water and acetone with 500 μJ pulse energy. In the former, the optimum fitting using Mie's theory yielded a dominant core radius $R = 0.9$ nm with a shell thickness distribution of 40% R and 150% R, while in the latter there is a larger size dispersion with a dominant size of Cu bare core 2 nm radius together with a small abundance of Cu-Cu$_2$O 10 nm particles as well as an important subnanometric contribution of 0.8 nm core radius of the same configuration. We also showed that the method of spectral fitting is extremely sensitive to small variations in core radius (± 0.1 nm) or shell thickness ($\pm 20\%$ R). These small changes modify the shape of the curves and depart from the experimental spectrum.

For comparison purposes the colloidal suspensions generated by fs laser ablation were analyzed with standard microscopy techniques such as AFM and HRTEM. The results show very good agreement with those obtained from the fitting of the experimental extinction spectra using the Drude-interband model.

OES can be applied thus as a complementary method to advanced microscopy techniques for sizing spherical bare core and core-shell metal Nps in the nanometer-subnanometer size range. Besides, OES allows to determine the structure (bare core or core-shell) of the Nps present in the colloidal solution as well as its abundance. It also has the advantage of providing a very good measurement statistics due to the large number of particles in the path of the spectrophotometer beam across the sample cell. Besides, it avoids coalescence effects since the measurement is made directly on the colloidal suspension.

ACKNOWLEDGMENTS

[1]H. Wang, Y. Huang, Z. Tan, and X. Hu, "Fabrication and characterization of copper nanoparticle thin-films and the electrocatalytic behavior," Anal. Chim. Acta **526**, 13–17 (2004).

[2]G. Larsen and S. Noriega, "Dendrimer-mediated formation of Cu-CuO$_x$ nanoparticles on silica and their physical and catalytic characterization," Appl. Catal. A: Gen. **278**, 73–81 (2004).

[3]H. Zhu, C. Zhang, and Y. Yin, "Novel synthesis of copper nanoparticles: influence of the synthesis conditions on the particle size," Nanotechnology **16**, 3079 (2005).

[4]M. K. Patel, B. J. Nagare, D. M. Bayul, S. K. Haram, and D. C. Kothari, "Controlled synthesis of Cu nanoparticles in fused silica and BK7 glasses using ion beam induced defects," Surf. Coat. Technol. **196**, 96–99 (2005).

[5]J. A. Dieringer, A. D. McFarland, N. C. Shah, D. A. Stuart, A. V. Whitney, C. R. Yonson, M. A. Young, X. Zhang, and R. P. Van Duyne, "Surface enhanced Raman spectroscopy: New materials, concepts, characterization tools, and applications," Faraday Discuss **132**, 9–26 (2006).

[6]J. Zhao, A. Das, X. Zhang, G. C. Schatz, S. G. Sligar, and R. P. Van Duyne, "Resonance surface plasmon spectroscopy: Low molecular weight substrate binding to cytochrome P450," J. Am. Chem. Soc. **128**, 11004–11005 (2006).

[7]A. M. Moran, J. Sung, E. M. Hicks, R. P. Van Duyne, and G. K. Spears, "Second harmonic excitation spectroscopy of silver nanoparticle arrays," J. Phys. Chem. B **109**, 4501–4506 (2005).

[8]A. J. Haes, W. P. Hall, L. Chang, W. L. Klein, and R. P. Van Duyne, "A localized surface plasmon resonance biosensor: First steps toward an assay for Alzheimer's disease," Nano Lett. **4**, 1029–1034 (2004).

[9]J. Jiang, K. Bosnick, M. Maillard, and L. Brus, "Single molecule raman spectroscopy at the junctions of large Ag nanocrystals," J. Phys. Chem. B **107**, 9964–9972 (2003).

[10]A. Quaranta, R. Ceccato, C. Menato, L. Pederiva, N. Capra, and R. Dal Maschio, "Formation of copper nanocrystals in alkali-lime silica glass by means of different reducing agents," J. Non-Cryst. Solids **345–346**, 671–675 (2004).

[11]T. N. Rostovshchikov, V. V. Smirnov, V. M. Kozhevin, D. A. Yavsin, M. A. Zabelin, I. N. Yassievich, and S. A. Gurevich, "New size effect in the catalysis by interacting copper nanoparticles," Appl. Catal. A Gen. **296**, 70–79 (2005).

[12]Y. Gotoh, R. Igarashi, Y. Ohkoshi, M. Nagura, K. Akamatsu, and S. Deki, "Preparation and structure of copper nanoparticle/poly(acrylicacid) composite films," J. Mater. Chem. **10**, 2548–2552 (2000).

[13]V. A. Bogatyrev, L. A. Dykman, B. N. Khlebtsov, and N. G. Khlebtsov, "Measurement of mean size and evaluation of polydispersity of gold nanoparticles from spectra of optical absorption and scattering," Opt. Spectrosc. **96**, 128–135 (2004).

[14]L. B. Scaffardi and J. O. Tocho, "Size dependence of refractive index of gold nanoparticles," Nanotechnology **17**, 1309–1315 (2006).

[15]M. V. Roldán, L. B. Scaffardi, O. de Sanctis, and N. Pellegri, "Optical properties and extinction spectroscopy to characterize the synthesis of amine capped silver nanoparticles," Mater. Chem. Phys. **112**, 984–990 (2008).

[16]D. C. Schinca and L. B. Scaffardi, "Core and shell sizing of small silver coated nanospheres by optical extinction spectroscopy," Nanotechnology **19**, 495712 (2008).

[17]D. C. Schinca, L. B. Scaffardi, F. A. Videla, G. A. Torchia, P. Moreno, and L. Roso, "Silver-silver oxide core-shell nanoparticles by femtosecond laser ablation: Core and shell sizing by extinction spectroscopy," J. Phys. D: Appl. Phys. **42**, 215102 (2009).

[18]J. M. J. Santillán, L. B. Scaffardi, and D. C. Schinca, "Quantitative optical extinction-based parametric method for sizing a single core-shell Ag-Ag$_2$O nanoparticle," J. Phys. D: Appl. Phys. **44**, 105104 (2011).

[19]A. Pinchuk, G. von Plessen, and U. Kreibig, "Influence of interband electronic transitions on the optical absorption in metallic nanoparticles," J. Phys. D: Appl. Phys. **37**, 3133–9 (2004).

[20]H. Inouye, K. Tanaka, I. Tanahashi, and K. Hirao, "Ultrafast dynamics of nonequilibrium electrons in a gold nanoparticle system," Phys. Rev. B **57**, 11334–40 (1998).

[21]S. L. Logunov, T. S. Ahmadi, M. A. El-Sayed, J. T. Khoury, and R. L. Whetten, "Electron dynamics of passivated gold nanocrystals probed by subpicosecond transient absorption spectroscopy," J. Phys. Chem. B **101**, 3713–9 (1997).

[22]P. B. Johnson and R. W. Christy "Optical constants of the noble metals," Phys. Rev. B **6**, 4370–9 (1972).

[23]W. Cai and V. Shalaev, *Optical Metamaterials. Fundamentals and Applications* (Springer, Berlin, 2010).

[24]G. W. C. Kaye and T. H. Laby, *Tables of Physical and Chemical Constants and Some Mathematical Functions* (Longman Scientific and Technical, London, 1995).

[25]U. Kreibig and M. Vollmer, *Optical Properties of Metal Clusters* (Springer, Berlin, 1995).

[26]C. F. Bohren and D. R. Huffman, *Absorption and Scattering of Light by Small Particles* (Wiley, New York, 1998).

[27]*Handbook of Optical Constants of Solids*, edited by E. D. Palik (Academic, New York, 1998), Vol. 1.